Journal of Molecular Spectroscopy **204,** 125–132 (2000)
doi:10.1006/jmsp.2000.8186, available online at http://www.idealibrary.com on IDEAL®

Laser-Induced Fluorescence and Fourier Transform Spectroscopy of NiCl: Identification of a Low-Lying $^2\Sigma^+$ State (1768 cm^{-1})

A. Poclet,* Y. Krouti,*,[1] T. Hirao,† B. Pinchemel,* and P. F. Bernath†

*Laboratoire de Physique des Lasers, Atomes et Molécules, UMR CNRS 8523, Centre d'Etudes et de Recherches Laser et Applications, Université des Sciences et Technologies de Lille, 59655, Villeneuve d'Ascq Cedex, France; and †Department of Chemistry, University of Waterloo, Waterloo, Ontario, Canada N2L 3G1

Received May 22, 2000

From a comparison with the spectrum of NiF, a low-lying $^2\Sigma^+$ state is expected to lie in the first 2000 cm^{-1} above the ground $X^2\Pi_{3/2}$ state of NiCl. The identification of this $^2\Sigma^+$ ($v = 0$) state (at 1768 cm^{-1}) has been carried out through the analysis of two electronic transitions $^2\Pi_{3/2}$–$^2\Sigma^+$ (22 720 cm^{-1}) and $^2\Pi_{1/2}$–$^2\Sigma^+$ (23 210 cm^{-1}) recorded by high-resolution Fourier transform spectroscopy. Dispersed fluorescence spectroscopy allowed these transitions to be located on an absolute energy-level diagram that includes the previously studied electronic states.

I. INTRODUCTION

In a recent paper (*1*) the $X^2\Pi_{3/2}$ ($v = 0$) and the $[0.16]A^2\Delta_{5/2}$ ($v = 0$) spin–orbit components of the low-lying electronic states of $^{58}Ni^{35}Cl$ have been found through the rotational analysis of two electronic transitions linking these states to a common upper $^2\Delta_{5/2}$ ($v = 0$) state located at 21 905 cm^{-1}. Comparison with the isovalent molecule NiF (*2*) suggests that a low-lying $^2\Sigma^+$ state must be observed in the vicinity of the $X^2\Pi_i$ and $A^2\Delta_i$ states. Each of these states is associated, respectively, with $\sigma\pi^4\delta^4$, $\sigma^2\pi^3\delta^4$, and $\sigma^2\pi^4\delta^3$ molecular electronic configurations, correlating with the $3d$ atomic orbital on the nickel atom (*3*). The states correspond to $3d\sigma^{-1}$, $3d\pi^{-1}$, $3d\delta^{-1}$ electron holes on the nickel atom. Selection rules prevent the observation of any transition between the known upper $^2\Delta_{5/2}$ state and a $^2\Sigma$ state. To observe such a $^2\Sigma$ state it was necessary to identify first a $^2\Pi$ (or a $^2\Sigma$) excited state and in a second step to locate and analyze a possible $^2\Pi$–$^2\Sigma$ (or a $^2\Sigma$–$^2\Sigma$) transition.

The emission spectrum of NiCl is rather dense in the visible spectral region and, except for the two previously analyzed bands (*1*), the bands are often overlapped and have only a modest signal-to-noise ratio in our spectra. In addition Ni atomic lines, emitted by the microwave discharge, frequently overlap the spectral regions of interest. Low-resolution fluorescence experiments provided useful information to build an energy-level diagram leading to the identification of a new excited $^2\Pi_i$ state, the $\Omega = \frac{3}{2}$ spin–orbit component of which is linked to the $X^2\Pi_{3/2}$ and the $A^2\Delta_{5/2}$ states. Both the $\Omega = \frac{3}{2}$ (24 490 cm^{-1}) and the $\Omega = \frac{1}{2}$ (24 975 cm^{-1}) spin components are linked to a $^2\Sigma^+$ state (1768 cm^{-1}). The identification of these transitions has been helped by the observation of a weak forbidden transition between the upper $^2\Pi_{1/2}$ state and the $X^2\Pi_{3/2}$ ground state (Fig. 1).

High-resolution Fourier transform experiments provided spectra which have been rotationally analyzed and identified as the $^2\Pi_{3/2}$–$^2\Sigma^+$ (22 720 cm^{-1}) and the $^2\Pi_{1/2}$–$^2\Sigma^+$ (23 210 cm^{-1}) transitions. This work thus reports on a new low-lying $^2\Sigma^+$ state located at 1768 cm^{-1} above the ground $^2\Pi_{3/2}$ state.

II. EXPERIMENTAL DETAILS

Both fluorescence and Fourier transform experiments have been described in a previous paper (*1*). In the laser-induced fluorescence experiments, nickel vapor produced in a heated graphite tube reacts with CH_3Cl to produce NiCl. The laser beam of a broadband cw dye laser (Coherent 699-01) running with stylbene 3 dye interacts with the molecules, and the resultant fluorescence signal is focused on the entrance slit of a spectrometer. The dispersed light is recorded by a photomultiplier tube using a lock-in amplifier and a chart recorder.

The Fourier transform emission spectra were recorded with a Bruker IFS 120 HR spectrometer. Heated $NiCl_2$ vapor is carried by He buffer gas in a quartz tube located inside a 2450 MHz microwave discharge. Spectra from 19 800 to 26 500 cm^{-1} were recorded with a visible quartz beamsplitter. To eliminate strong atomic lines and to narrow the wavelengths region to improve the signal-to-noise ratio, we inserted a 500-nm blue-pass filter (Corion LS-500) in front of the photomultiplier tube. In total 10 scans were accumulated in 10 min at a spectral resolution of 0.03 cm^{-1}. The signal-to-noise ratio was about 10 and the typical linewidth was 0.07 cm^{-1}. The accuracy of line positions was estimated to be better than 0.007 cm^{-1}.

The spectrometer was not evacuated, so all line positions were corrected for the refractive index of air (*4*, *5*). To convert

[1] Permanent address: Laboratoire de Physique Atomique & Moléculaire, Faculté des Sciences Aïn Chock B.P. 5366 Maârif, Casablanca, Morocco.

0022-2852/00 $35.00

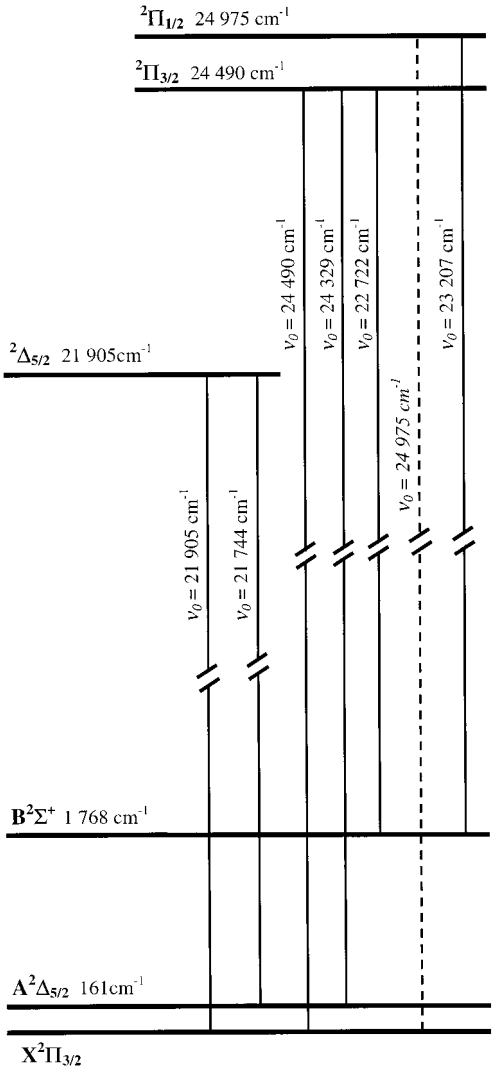

FIG. 1. Energy-level diagram of the observed transitions of NiCl including the two transitions $[21.9]^2\Delta_{5/2}$–$X^2\Pi_{3/2}$ and $[21.9]^2\Delta_{5/2}$–$[0.16]A^2\Delta_{5/2}$ analyzed in Ref. (*1*). The energies are T_0 values and the dashed line is the unanalyzed forbidden transition $[24.9]^2\Pi_{1/2}$–$X^2\Pi_{3/2}$.

the line positions to vacuum wavenumbers, we applied the polynomial expression obtained using Edlén's formula (*6*)

$$\Delta = \tilde{\nu}_{\text{ex}} - 15\,000, \qquad [1]$$

$$\begin{aligned}\delta = &-6.619702 \times 10^{-3} + 6.7274390 \times 10^{-6} \times \Delta \\ &+ 7.367955 \times 10^{-10} \times \Delta^2 + 1.864215 \times 10^{-14} \\ &\times \Delta^3 + 1.22781 \times 10^{-19} \times \Delta^4 + 2.46704 \times 10^{-24} \\ &\times \Delta^5 + 2.8993 \times 10^{-29} \times \Delta^6, \qquad [2]\end{aligned}$$

$$\tilde{\nu}_{\text{vac}} = \tilde{\nu}_{\text{ex}} - \delta, \qquad [3]$$

where $\tilde{\nu}_{\text{ex}}$ is the measured spectral position in reciprocal centimeter units in the atmosphere assuming that the standard internal He–Ne laser emits exactly at 15 798 cm^{-1}, and $\tilde{\nu}_{\text{vac}}$ indicates the vacuum wavenumber. Calibration was carried out using He atomic lines present in our spectra. Standard He line positions were determined in a separate experiment with He/Ar mixture with the Ar lines taken from the literature (*7*), and the calibration factor was 1.00000223.

III. DESCRIPTION OF THE ELECTRONIC STATES LINKED BY FLUORESCENCE EXPERIMENTS

In a first step, fluorescence experiments showed that an electronic state located at 24 490 cm^{-1} was linked to the $X^2\Pi_{3/2}$ and the $[0.16]A^2\Delta_{5/2}$ states. In addition an intense fluorescence signal was observed at 22 720 cm^{-1}, suggesting the presence of a new electronic state located at 1768 cm^{-1} above the ground state. Among the numerous bands probed when the laser was tuned to a bandhead situated at 23 210 cm^{-1} was a weak-induced fluorescence signal at 24 980 cm^{-1}, i.e., 1770 cm^{-1} to the blue of the laser-excited transition. In the first experiment the upper state has been considered to be a $[24.5]^2\Pi_{3/2}$ state linked to the $X^2\Pi_{3/2}$ state (24 490 cm^{-1} transition), to the $[0.16]A^2\Delta_{5/2}$ state (24 330 cm^{-1} transition), and to a new $^2\Sigma^+$ state (22 720 cm^{-1} transition). The second fluorescence experiment suggests that a $[24.9]^2\Pi_{1/2}$ state is the upper state of a $[24.9]^2\Pi_{1/2}$–$X^2\Pi_{3/2}$ forbidden transition (24 977 cm^{-1}) and of a transition (23 210 cm^{-1}) connecting to the same new $^2\Sigma$ state. All these states and the associated transitions are drawn on an energy-level diagram (Fig. 1). These assumptions about the nature of the transitions have been confirmed by the study of the high-resolution spectra provided by Fourier transform spectroscopy experiments: the characteristic pattern of a $^2\Pi$–$^2\Sigma$ transition was observed for both the 22 720 cm^{-1} (Fig. 2) and the 23 210 cm^{-1} transition. In addition the occurrence of Q branches has been checked in order to support the nature of the states in the other observed transitions involving the $X^2\Pi_{3/2}$ and the $[0.16]A^2\Delta_{5/2}$ states.

A general survey of the 19 800–26 300 cm^{-1} spectral region shows that the high quality of the recordings of the two bands (21 750 and 21 905 cm^{-1}) recently published (*1*) is not obtained for the other bands. The signal-to-noise ratio is only moderate for the new bands analyzed in the present work, and this leads to intensity alterations which make it difficult in some cases to identify the lines belonging to a branch. In addition some branches of the new transitions are missing and there are numerous nickel atomic lines that severely overlap the rotational structure. As a consequence, a step-by-step procedure has been followed in the work. We started the analysis of a band only when the rotational constants and (if needed) the fine-structure constants of one of the two involved states were known from a previously analyzed transition.

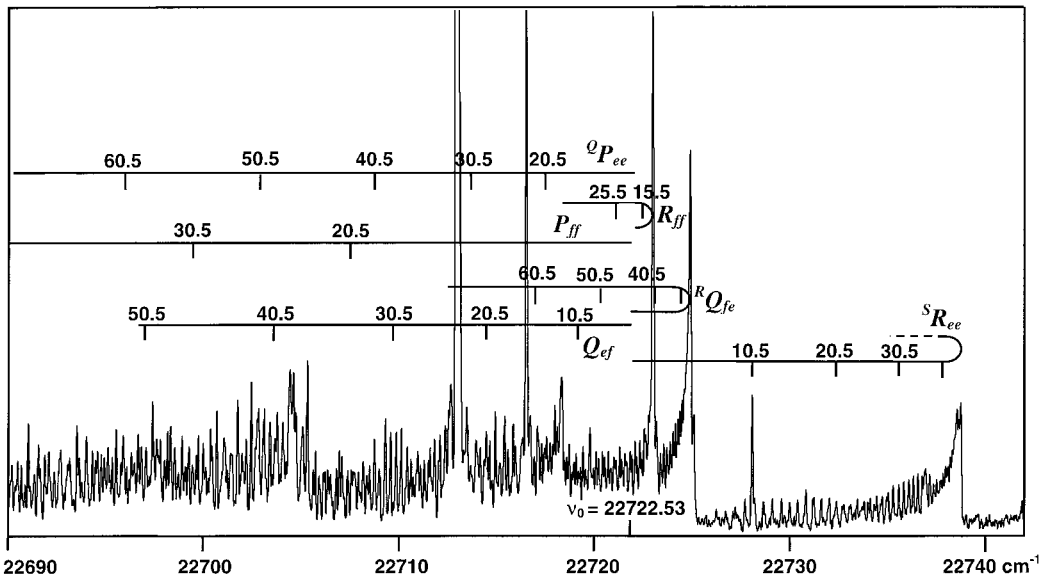

FIG. 2. The $[24.5]^2\Pi_{3/2}$ ($v = 0$)–$[1.7]^2\Sigma^+$ ($v = 0$) transition of NiCl.

IV. ROTATIONAL ANALYSIS OF THE $[24.5]^2\Pi_{3/2}$–$[0.16]A^2\Delta_{5/2}$ (24 330 cm^{-1}) AND OF THE $[24.5]^2\Pi_{3/2}$–$X^2\Pi_{3/2}$ (24 490 cm^{-1}) TRANSITIONS

The analysis of these two transitions was straightforward because the parameters of the $[0.16]A^2\Delta_{5/2}$ and $X^2\Pi_{3/2}$ states are now well known (*1*). In the $[24.5]^2\Pi_{3/2}$–$[0.16]A^2\Delta_{5/2}$ transition, three branches Q ($J = 9.5$ to $J = 77.5$), P ($J = 9.5$ to $J = 76.5$), and R ($J = 23.5$ to $J = 62.5$) allowed for an easy determination of the parameters of the upper state. Despite the high J values reached in the Q and P branches, no splitting of the lines was in evidence. One can conclude that there is no Λ-doubling in the $[24.5]^2\Pi_{3/2}$ spin–orbit component.

The second transition $[24.5]^2\Pi_{3/2}$–$X^2\Pi_{3/2}$ (24 490 cm^{-1}) is more congested because of the presence of a splitting proportional to J^3 in the ground $X^2\Pi_{3/2}$ state (*1*). As a consequence, two branches R_{ee} and R_{ff} ($J = 32.5$ to $J = 68.5$) have been found and the splitting of the lines starts at $J = 38.5$. Only one P branch is observed between $J = 10.5$ and $J = 30.5$. A fit of the two transitions using the classical effective expressions (*8*) to characterize the terms values of the three states led to accurate values of the rotational B and centrifugal distortion D parameters for the upper $[24.5]^2\Pi_{3/2}$ state. These reliable term values for this state was the key to the analysis of the $[24.5]^2\Pi_{3/2}$–$[1.7]^2\Sigma^+$ transition.

In addition it has been possible to rotationally analyze the 0–1 (23 900.7 cm^{-1}) and 1–0 (24 737.4 cm^{-1}) bands of the $[24.5]^2\Pi_{3/2}$–$[0.16]A^2\Delta_{5/2}$ transition, the lines of which are collected in Table 1. The derived parameters from a fit using a polynomial description (*8*) for the $v = 1$ level of the $[24.5]^2\Pi_{3/2}$ are $T_1 = 24\,895.613(3)$ cm^{-1}, $B_1 = 0.173688(30)$ cm^{-1}, and $D_1 = 1.185(20) \times 10^{-7}$ cm^{-1}.

V. ROTATIONAL ANALYSIS OF THE $[24.5]^2\Pi_{3/2}$–$[1.7]^2\Sigma^+$ TRANSITION (22 720 cm^{-1})

The pattern of this band (Fig. 2) is characteristic of a transition between a (Hund's case *a*) $^2\Pi$ state and a (Hund's case *b*) $^2\Sigma$ state (*8*). The head-forming $^{S}R_{ee}$ branch is easy to identify because of its widely spaced rotational structure. The $^{R}Q_{fe}$ head is also clearly visible but the R_{ff} head is overlapped by an intense nickel atomic line. In absence of any Λ-doubling in the upper $[24.5]^2\Pi_{3/2}$ state, the *e*- and *f*-parity levels of this state are degenerate. The exact J numbering of the $^{S}R_{ee}$ and the $^{R}Q_{fe}$ branches was easily determined from the calculation of the *e*-parity term values of the lower $^2\Sigma^+$ state derived from the differences between the upper state term values determined in Section IV and the experimental wavenumbers of the lines of these two branches. A good estimate of the B'', D'', and of the spin–rotation parameter γ'' was derived and then the lines of the $^{Q}P_{ee}$ branch were picked out. The congestion in the spectrum made it difficult to identify lines linking the degenerate term values of the upper $[24.5]^2\Pi_{3/2}$ state to the *f*-parity term values of the $^2\Sigma^+$ state. Moreover, it was obvious that the spin–rotation parameter γ was not accurately determined in a fit which did not include any lines involving the *f*-parity levels of the lower $^2\Sigma^+$ state. At this stage of the study, no reliable estimate of a γ_D parameter accounting for a centrifugal distortion on the spin–rotation contribution was possible.

Ultimately, the estimated term values of the *f*-parity levels of the $[1.7]^2\Sigma^+$ lower state led to the identification of some lines in the R_{ff}, Q_{ef}, and P_{ff} branches, which were then progressively included in the fit, keeping fixed the parameters of the upper $[24.5]^2\Pi_{3/2}$ state. A satisfying set of parameters for the lower $[1.7]^2\Sigma^+$ state has been derived leading to the determination of

TABLE 1

Observed Line Positions (in cm^{-1}) for the $[24.5]^2\Pi_{3/2}$ ($v = 0$)–$[0.16]A^2\Delta_{5/2}$ ($v = 0$), $[24.5]^2\Pi_{3/2}$ ($v = 0$)–$X^2\Pi_{3/2}$ ($v = 0$), $[24.5]^2\Pi_{3/2}$ ($v = 0$)–$[1.7]^2\Sigma^+$ ($v = 0$), $[24.9]^2\Pi_{1/2}$ ($v = 0$)–$[1.7]^2\Sigma^+$ ($v = 0$), $[24.5]^2\Pi_{3/2}$ ($v = 0$)–$[0.16]A^2\Delta_{5/2}$ ($v = 1$), and $[24.5]^2\Pi_{3/2}$ ($v = 1$)–$[0.16]A^2\Delta_{5/2}$ ($v = 0$) Transitions of $^{58}Ni^{35}Cl$

$[24.5]^2\Pi_{3/2}(0) - [0.16]A^2\Delta_{5/2}(0)$				$[24.5]^2\Pi_{3/2}(0) - X^2\Pi_{3/2}(0)$			$[24.5]^2\Pi_{3/2}(0) - [0.16]A^2\Delta_{5/2}(0)$				$[24.5]^2\Pi_{3/2}(0) - X^2\Pi_{3/2}(0)$		
J	R	Q	P	R_{ff}	R_{ee}	P	J	R	Q	P	R_{ff}	R_{ee}	P
9.5		24327.838	24324.498				44.5	24326.342	24310.495	24294.987	24492.612	24492.531	
10.5		24327.658	24323.964			24485.811	45.5	24325.879	24309.688	24293.828	24492.366	24492.251	
11.5		24327.458	24323.409			24485.310	46.5	24325.383	24308.837	24292.632	24492.100	24491.990	
12.5		24327.231	24322.832			24484.767	47.5	24324.862	24307.988	24291.438	24491.796	24491.667	
13.5		24326.977	24322.269			24484.287	48.5	24324.369	24307.116	24290.219	24491.510	24491.382	
14.5		24326.716	24321.655			24483.707	49.5	24323.812	24306.234	24288.987	24491.194	24491.067	
15.5		24326.434	24321.014			24483.160	50.5	24323.250	24305.324	24287.743	24490.880	24490.734	
16.5		24326.124	24320.379			24482.615	51.5	24322.649	24304.405	24286.465	24490.542	24490.378	
17.5		24325.813	24319.696			24481.977	52.5	24322.087	24303.463	24285.179	24490.196	24490.004	
18.5		24325.485	24319.030			24481.403	53.5	24321.462	24302.502	24283.863	24489.821	24489.650	
19.5		24325.130	24318.315			24480.815	54.5	24320.813	24301.527	24282.553	24489.438	24489.268	
20.5		24324.763	24317.602			24480.176	55.5	24320.204	24300.533	24281.218	24489.035	24488.834	
21.5		24324.369	24316.867			24479.520	56.5	24319.504	24299.494	24279.854	24488.625	24488.416	
22.5		24323.964	24316.112			24478.887	57.5		24298.493	24278.496	24488.234	24487.978	
23.5	24332.120	24323.542	24315.315			24478.230	58.5	24318.133	24297.450	24277.094	24487.758	24487.548	
24.5	24332.019	24323.100	24314.554			24477.546	59.5	24317.433	24296.370	24275.670	24487.325	24487.078	
25.5	24331.907	24322.649	24313.745			24476.857	60.5	24316.682	24295.299	24274.250	24486.841	24486.627	
26.5	24331.766	24322.156	24312.901			24476.164	61.5	24315.942	24294.198	24272.828	24486.377	24486.117	
27.5	24331.626	24321.655	24312.077			24475.443	62.5	24315.142	24293.083	24271.365	24485.922	24485.610	
28.5	24331.466	24321.151	24311.186			24474.707	63.5		24291.948	24269.868	24485.388	24485.101	
29.5	24331.283	24320.617	24310.308			24473.976	64.5		24290.781	24268.397	24484.884	24484.586	
30.5	24331.076	24320.068	24309.418			24473.189	65.5		24289.615	24266.859	24484.353	24484.027	
31.5	24330.862	24319.504	24308.504				66.5		24288.434	24265.339	24483.827	24483.466	
32.5	24330.611	24318.907	24307.579	24494.697	24494.697		67.5		24287.229	24263.788	24483.265	24482.880	
33.5	24330.358	24318.315	24306.617	24494.578	24494.578		68.5		24286.013	24262.235	24482.693		
34.5	24330.083	24317.686	24305.670	24494.456	24494.456		69.5		24284.773	24260.666			
35.5	24329.790	24317.051	24304.661	24494.329	24494.329		70.5		24283.513	24259.048			
36.5	24329.481	24316.392	24303.661	24494.194	24494.194		71.5		24282.229	24257.430			
37.5	24329.163	24315.719	24302.640	24494.040	24494.040		72.5		24280.947	24255.790			
38.5	24328.802	24315.028	24301.607	24493.876	24493.825		73.5		24279.659	24254.159			
39.5	24328.436	24314.325	24300.533	24493.688	24493.640		74.5		24278.326	24252.481			
40.5	24328.047	24313.590	24299.494	24493.511	24493.476		75.5		24276.992	24250.794			
41.5	24327.658	24312.852	24298.365	24493.307	24493.232		76.5		24275.641	24249.116			
42.5	24327.231	24312.077	24297.239	24493.124	24493.006		77.5		24274.250				
43.5	24326.794	24311.302	24296.135	24492.857	24492.778								

$[24.5]^2\Pi_{3/2}(0) - [1.7]^2\Sigma^+(0)$							$[24.5]^2\Pi_{3/2}(0) - [1.7]^2\Sigma^+(0)$						
J	$^sR_{ee}$	R_{ff}	$^RQ_{fe}$	Q_{ef}	$^QP_{ee}$	Pff	J	$^sR_{ee}$	R_{ff}	$^RQ_{fe}$	Q_{ef}	$^QP_{ee}$	Pff
3.5				22721.069			36.5	22736.888		22723.831	22706.317	22711.076	22693.596
4.5				22720.798			37.5	22737.091		22723.661	22705.695	22710.587	22692.596
5.5	22725.620			22720.487			38.5	22737.278		22723.498	22705.040	22710.076	22691.628
6.5	22726.154			22720.163			39.5	22737.443		22723.328		22709.527	22690.638
7.5	22726.659						40.5	22737.613		22723.133	22703.749	22708.991	22689.624
8.5	22727.155						41.5	22737.762			22703.086	22708.459	22688.619
9.5	22727.646			22719.236			42.5	22737.913		22722.739	22702.415	22707.902	22687.570
10.5	22728.128			22718.912			43.5	22738.024		22722.514	22701.724	22707.347	22686.551
11.5	22728.602			22718.540			44.5	22738.135		22722.284	22701.039	22706.765	22685.526
12.5	22729.066						45.5	22738.229		22722.041	22700.327	22706.185	22684.486
13.5	22729.505			22717.806			46.5			22721.786	22699.603	22705.581	22683.369
14.5	22729.951	22722.815		22717.377			47.5			22721.528	22698.879		22682.336
15.5	22730.355						48.5			22721.248	22698.130		22681.253
16.5	22730.772	22722.739			22718.912		49.5			22720.973	22697.373	22703.749	22680.164
17.5	22731.201			22716.177	22718.657		50.5			22720.679		22703.086	22679.036
18.5	22731.579	22722.587		22715.783			51.5			22720.376		22702.415	22677.916
19.5	22731.970			22715.352	22718.024		52.5			22720.042		22701.724	22676.802
20.5	22732.338	22722.373		22714.879	22717.664	22707.713	53.5			22719.728		22701.099	22675.656
21.5	22732.713	22722.284		22714.411	22717.377	22706.922	54.5			22719.378		22700.419	22674.518
22.5	22733.068	22722.131			22717.024	22706.093	55.5			22719.023		22699.713	22673.333
23.5	22733.406	22722.041			22716.660	22705.284	56.5			22718.657		22699.013	22672.183
24.5	22733.735	22721.878			22716.261		57.5			22718.257		22698.276	22670.993
25.5	22734.066			22712.498	22715.910		58.5			22717.910		22697.567	22669.816
26.5	22734.368			22711.985	22715.518	22702.720	59.5			22717.501		22696.797	22668.607
27.5	22734.682			22711.466	22715.139	22701.861	60.5			22717.087		22696.045	22667.412
28.5	22734.966			22710.931	22714.719		61.5			22716.660		22695.303	22666.195
29.5	22735.230		22724.618	22710.390	22714.313	22700.085	62.5			22716.226		22694.529	22664.958
30.5	22735.507		22724.532	22709.828	22713.892	22699.186	63.5			22715.785		22693.735	22663.701
31.5	22735.760		22724.436	22709.270	22713.415	22698.276	64.5			22715.352		22692.928	22662.455
32.5	22736.029		22724.331	22708.709		22697.373	65.5			22714.879		22692.134	22661.194
33.5	22736.261		22724.225	22708.139	22712.498	22696.420	66.5			22714.411		22691.306	22659.914
34.5	22736.496		22724.098	22707.532	22712.056	22695.497	67.5			22713.892		22690.459	22658.632
35.5	22736.702		22723.973	22706.922	22711.570	22694.530	68.5			22713.415		22689.624	22657.336

TABLE 1—*Continued*

$[24.9]^2\Pi_{1/2}(0) - [1.7]^2\Sigma^+(0)$					$[24.9]^2\Pi_{1/2}(0) - [1.7]^2\Sigma^+(0)$				
J	R_{ee}	Q_{fe}	$^PQ_{ef}$	$^OP_{ff}$	J	R_{ee}	Q_{fe}	$^PQ_{ef}$	$^OP_{ff}$
4.5				23204.154	47.5		23206.845	23183.258	23167.634
5.5	23210.465			23203.521	48.5		23206.574		23166.553
6.5	23210.959			23202.896	49.5		23206.313	23181.718	23165.471
7.5	23211.445			23202.238	50.5			23180.935	23164.354
8.5	23211.955			23201.580	51.5		23205.718	23180.152	23163.253
9.5	23212.413			23200.911	52.5		23205.399	23179.397	23162.135
10.5	23212.893			23200.216	53.5		23205.082		23160.992
11.5	23213.334			23199.540	54.5		23204.732		23159.865
12.5	23213.802			23198.814	55.5		23204.394		23158.701
13.5	23214.230			23198.130	56.5		23204.032		23157.547
14.5	23214.649			23197.372	57.5		23203.658		23156.367
15.5	23215.060			23196.635	58.5		23203.270		23155.175
16.5	23215.465			23195.890	59.5		23202.886		23153.993
17.5	23215.875			23195.133	60.5		23202.481		23152.806
18.5	23216.245			23194.367	61.5		23202.073		23151.565
19.5	23216.649			23193.588	62.5		23201.639		23150.337
20.5	23216.985			23192.792	63.5				23149.107
21.5	23217.367			23192.004	64.5				23147.849
22.5	23217.686			23191.201	65.5				23146.592
23.5	23218.021			23190.379	66.5				23145.320
24.5	23218.345			23189.556	67.5				23144.028
25.5	23218.663			23188.723	68.5				23142.748
26.5	23218.937			23187.865	69.5				23141.448
27.5	23219.242			23187.009	70.5				23140.127
28.5	23219.521			23186.132	71.5				23138.813
29.5	23219.798			23185.262	72.5				23137.476
30.5	23220.050	23209.695		23184.362	73.5				23136.120
31.5	23220.294			23183.465	74.5				23134.747
32.5	23220.554	23209.550		23182.553	75.5				23133.389
33.5	23220.777	23209.429		23181.628	76.5				23132.008
34.5	23220.985	23209.281		23180.697	77.5				23130.630
35.5	23221.177		23191.457	23179.754	78.5				23129.220
36.5	23221.377	23209.062	23190.797	23178.807	79.5				23127.812
37.5	23221.554	23208.896	23190.135		80.5				23126.393
38.5	23221.730	23208.736	23189.556	23176.876	81.5				23124.946
39.5	23221.883		23188.882	23175.887	82.5				23123.513
40.5	23222.050	23208.409	23188.174	23174.885	83.5				23122.036
41.5	23222.181	23208.224		23173.892	84.5				23120.569
42.5	23222.294	23208.009	23186.827	23172.865	85.5				23119.102
43.5	23222.408	23207.800	23186.132	23171.835	86.5				23117.613
44.5	23222.512	23207.574	23185.401	23170.805	87.5				23116.096
45.5	23222.621	23207.337	23184.707	23169.756	88.5				23114.582
46.5		23207.103	23183.986	23168.698					

$[24.5]^2\Pi_{3/2}(0) - [0.16]A^2\Delta_{5/2}(1)$				$[24.5]^2\Pi_{3/2}(1) - [0.16]A^2\Delta_{5/2}(0)$			$[24.5]^2\Pi_{3/2}(0) - [0.16]A^2\Delta_{5/2}(1)$				$[24.5]^2\Pi_{3/2}(1) - [0.16]A^2\Delta_{5/2}(0)$		
J	R	Q	P	R	Q	P	J	R	Q	P	R	Q	P
7.5		23896.087					33.5	23899.476	23887.448	23875.747	24734.417	24722.454	24710.838
8.5		23895.961					34.5	23899.297	23886.915	23874.855	24734.058	24721.741	24709.798
9.5		23895.835				24729.772	35.5	23899.073	23886.339	23873.938	24733.698	24721.028	24708.739
10.5		23895.648				24729.191	36.5	23898.841	23885.766	23873.057		24720.308	24707.652
11.5		23895.445					37.5	23898.580	23885.164	23872.082	24732.898	24719.554	24706.557
12.5						24728.000	38.5	23898.346	23884.556	23871.132		24718.786	24705.419
13.5		23895.047			24732.111	24727.403	39.5		23883.946	23870.142	24732.065	24718.008	
14.5		23894.837			24731.794	24726.749	40.5	23897.763	23883.284	23869.146	24731.571	24717.189	24703.133
15.5		23894.574			24731.485	24726.101	41.5	23897.482	23882.647	23868.197		24716.338	24701.968
16.5		23894.318			24731.162	24725.411	42.5	23897.162	23881.976	23867.161		24715.508	24700.776
17.5		23894.034	23887.938		24730.802	24724.722	43.5	23896.779	23881.299	23866.120		24714.621	24699.563
18.5		23893.752	23887.258		24730.430	24724.024	44.5	23896.432	23880.593	23865.047		24713.730	24698.318
19.5		23893.440	23886.619	24737.145	24730.051	24723.279	45.5	23896.087	23879.863	23864.030		24712.826	24697.086
20.5		23893.106	23885.981	24737.099	24729.628	24722.508	46.5	23895.677	23879.156	23862.930		24711.888	24695.769
21.5		23892.768	23885.258	24737.018	24729.191	24721.741	47.5	23895.258	23878.379	23861.836		24710.939	24694.485
22.5		23892.417		24736.899	24728.745	24720.938	48.5		23877.624	23860.732		24709.975	24693.177
23.5		23892.036	23883.839	24736.759	24728.292	24720.128	49.5	23894.437	23876.848	23859.596		24708.995	24691.846
24.5		23891.662	23883.081	24736.614	24727.770	24719.285	50.5	23893.986	23876.044	23858.473		24707.985	24690.466
25.5		23891.271	23882.343	24736.465	24727.274	24718.434	51.5		23875.232	23857.299		24706.940	24689.105
26.5		23890.830	23881.576	24736.289	24726.749	24717.533	52.5		23874.422	23856.142		24705.893	24687.736
27.5		23890.384	23880.774	24736.069	24726.200	24716.638	53.5		23873.557	23854.924		24704.829	24686.288
28.5	23900.230	23889.925	23879.996	24735.853	24725.604	24715.760	54.5		23872.702	23853.702		24703.735	24684.885
29.5	23900.121	23889.490	23879.156	24735.608	24725.016	24714.772	55.5		23871.842	23852.523		24702.628	24683.435
30.5	23900.010	23888.992	23878.379	24735.336	24724.395	24713.832	56.5		23870.926	23851.278		24701.511	24681.954
31.5	23899.841	23888.490		24735.049	24723.761	24712.826	57.5		23870.063	23850.036		24700.353	24680.444
32.5	23899.679	23887.977	23876.639	24734.727	24723.125	24711.851	58.5		23869.146	23848.764		24699.180	24678.940

TABLE 1—*Continued*

$[24.5]^2\Pi_{3/2}(0) - [0.16]A^2\Delta_{5/2}(1)$				$[24.5]^2\Pi_{3/2}(1) - [0.16]A^2\Delta_{5/2}(0)$			$[24.5]^2\Pi_{3/2}(0) - [0.16]A^2\Delta_{5/2}(1)$				$[24.5]^2\Pi_{3/2}(1) - [0.16]A^2\Delta_{5/2}(0)$		
J	R	Q	P	R	Q	P	J	R	Q	P	R	Q	P
59.5		23868.197	23847.518		24698.002	24677.442	67.5					24687.793	24664.480
60.5		23867.207			24696.794	24675.869	68.5						24662.786
61.5		23866.246			24695.562	24674.332	69.5						24661.076
62.5		23865.274			24694.323	24672.710	70.5						24659.347
63.5		23864.301			24693.058	24671.094	71.5						
64.5					24691.768	24669.482	72.5						24655.779
65.5					24690.466	24667.843	73.5						24653.961
66.5					24689.152								

a γ_D parameter. Note that a final fit including all the studied transitions will be described in Section VII.

VI. ROTATIONAL ANALYSIS OF THE $[24.9]^2\Pi_{1/2}$–$[1.7]^2\Sigma^+$ TRANSITION (23 209 cm^{-1})

Once the term values of the $[1.7]^2\Sigma^+$ state were determined from the analysis described in Section V, it has been possible to study the $[24.9]^2\Pi_{1/2}$–$[1.7]^2\Sigma^+$ transition. The B and D constants of the upper state are expected to be close to the corresponding parameters calculated for the $[24.5]^2\Pi_{3/2}$ spin component. One can expect that a Λ-doubling splitting that increases linearly with J will be observed in the $\Omega = \frac{1}{2}$ upper state. Similar to the previously analyzed transition (Section V), the widely spaced rotational structure of the head-forming R_{ee} branch is observed from $J = 5.5$ to $J = 45.5$, and the ${}^OP_{ff}$ branch is also easy to follow from $J = 4.5$ to $J = 88.5$. (We note that lines of the corresponding P_{ff} branch of the $[24.5]^2\Pi_{3/2}$–$[1.7]^2\Sigma^+$ transition were difficult to pick out.) These R_{ee} and ${}^OP_{ff}$ branches can be fitted using the usual quadratic expression (*8*) in which the numbering of the lines is $m = J + 1$ in the R branch and $m = -J$ in the P branch. The large number of lines included in the fit and the knowledge of the constants of the lower $^2\Sigma^+$ state allows the determination of the B' parameter from the coefficient $(B' - B'')$ of the m^2 term of the polynomial. This value of $(B' - B'')$ is almost independent of the relative m numbering of the lines. In the polynomial expression, the linear m coefficient is equal to $(B' + 2B'' - \frac{1}{2}p' - \frac{1}{2}\gamma')$ and is strongly dependent on the numbering chosen in the fit. It turns out that even if the absolute numbering of the lines is known with an uncertainty no larger than ± 1, the value of the Λ-doubling parameter p' cannot be determined from this fit, despite the fact that B', B'', and γ' are known.

At this stage of the analysis, the Λ-doubling parameter p' could have three possible values, depending on the absolute numbering of the lines of the ${}^OP_{ff}$ and the R_{ee} branches included in the polynomial fit. In the spectral region close to the origin of the band, only one head is observed, which has been identified as the Q_{fe} branch. A second head-forming branch, ${}^QR_{ff}$ is expected to be found nearby but the contribution of γ and p to the linear m coefficient is large enough to force this branch to form its head at such a small m value that its intensity is not noticeable in this congested spectral region. A simulation of the Q_{fe} branch using the three possible values of p showed that the calculated positions of the head were 0.6 cm^{-1} away from the observation for two of the three possibilities. There was only one value of p (about -0.02 cm^{-1}) that produced agreement with the experimental position of the Q_{fe} head. It was then possible to identify lines from this Q_{fe} branch ($J = 30.5$ to $J = 62.5$) and some lines ($J = 35.5$ to $J = 52.5$) of the ${}^PQ_{ef}$ branch which were added to the fit of the $[24.9]^2\Pi_{1/2}$–$[1.7]^2\Sigma^+$ transition. No significant value of a centrifugal distortion parameter p'_D associated with the Λ-doubling parameter p' was in evidence.

VII. DETERMINATION OF THE CONSTANTS OF THE UPPER $^2\Pi_i$ STATE AND OF THE $[1.7]^2\Sigma^+$ STATE

In the previous sections several sets of constants have been determined from fits of the individual transitions using polynomial equations to account for the various electronic states involved. We can now include the 684 experimental lines (Table 1) in a single fit in which the four electronic states are described as follows.

The rotational Hamiltonians for the $[1.7]^2\Sigma^+$ and the upper $^2\Pi_i$ states have been accounted for by the well-known matrices given in Table 2 (*9*). In absence of information on the $X^2\Pi_{1/2}$ and $A^2\Delta_{3/2}$ spin–orbit components, the rotational Hamiltonians for the $X^2\Pi_{3/2}$ and $A^2\Delta_{5/2}$ levels have been represented by the polynomial expressions (*8*) already used in Ref. (*1*).

In the fitting procedure all the parameters of the $X^2\Pi_{3/2}$ and $A^2\Delta_{5/2}$ states have been kept fixed to the values determined in Ref. (*1*) except the band origins. The origin of the upper $^2\Pi_i$ state was also kept fixed and adjusted in order to make the T_0 value of the ground $X^2\Pi_{3/2}$ state to be at 0.00 cm^{-1}. The derived constants are listed in Table 3. The standard deviation on the lines is equal to 0.013 cm^{-1} despite the presence of many blended lines.

VIII. VIBRATIONAL ASSIGNMENT OF THE STUDIED TRANSITIONS

In addition to the rotational analyses already presented, the identification of some weak $\Delta v \neq 0$ vibrational bands has been possible. In most cases the 1–1 and even some 2–2 bandheads can be seen. From the knowledge of the vibrational parameters of the $X^2\Pi_{3/2}$ and $[0.16]A^2\Delta_{5/2}$ states (*1*), we have located some 0–1 bands, and from a crude estimate of the ω'_e value, we

TABLE 2
Matrices for $^2\Pi$ and $^2\Sigma$ Electronic States Derived Using Hund's Case (*a*) Basis Functions

$^2\Pi$ state

$\|J, 1/2, 3/2, e/f\rangle$	$\|J, -1/2, 1/2, e/f\rangle$
$T_O + A/2 + B_{3/2}[z-2] - D[z^2-3z+3]$	$-(z-1)^{1/2}[0.5(B_{1/2}+B_{3/2}) - 2D(z-1)] \mp 0.5q(z-1)^{1/2}(J+0.5)$
symmetric	$T_O - A/2 + B_{1/2}z - D[z^2+z-1] \pm 0.5(p+2q)(J+0.5)$

$z = (J+0.5)^2$, upper and lower signs refer to *e* and *f* rotational levels, respectively
The basis functions is $|J, \Sigma, \Omega, e/f\rangle$

$^2\Sigma$ state

$\|J, 1/2, e/f\rangle$
$T_O - \gamma/2 + Bz - D[z^2+z] \mp (B - \gamma/2 - 2Dz)(J+0.5) + \gamma_D/2[-2z \pm (z+1)(J+0.5)]$

$z = (J+0.5)^2$, upper and lower signs refer to *e* and *f* rotational levels, respectively
The basis functions is $|J, \Sigma, e/f\rangle$

have identified the 1–0 band of three of the four studied transitions. All of these bandhead positions are listed in Table 4. This table provides an estimate of $\Delta G_{1/2}$ for the newly studied states: $\Delta G_{1/2} = 405.1$ cm^{-1} for the $[24.5]^2\Pi_{3/2}$ state, $\Delta G_{1/2} = 401$ cm^{-1} for the $[24.9]^2\Pi_{1/2}$ state and $\Delta G_{1/2} = 425$ cm^{-1} for the $[1.7]^2\Sigma^+$ state. In the case of the $[24.5]^2\Pi_{3/2}$ ($v = 0$)–$[0.16]A^2\Delta_{5/2}$ ($v = 1$) transition, it has been possible to observe the bandheads of the three minor ^{60}Ni^{35}Cl, ^{58}Ni^{37}Cl, and ^{60}Ni^{37}Cl isotopomers. The position of these heads is in good agreement with the isotopic study presented in Ref. (*1*) and confirms the vibrational assignment of the studied transitions. One of the goals of this vibrational assignment is to reduce the number of unassigned bands of NiCl (now about 35) in the spectral range 19 800–26 200 cm^{-1} that we have recorded by Fourier transform spectroscopy.

IX. DISCUSSION AND CONCLUSION

The three low-lying states, $^2\Pi_i$, $^2\Delta_i$, and $^2\Sigma^+$, of NiCl are now firmly identified and we can make a comparison between the two isovalent molecules NiF and NiCl. In both cases the ground state is a $^2\Pi_i$ state and a $^2\Sigma^+$ state is observed at about the same position in respect with the ground state (1574 cm^{-1} for NiF and 1768 cm^{-1} for NiCl). Furthermore, γ spin–rotation parameters are of the same order of magnitude ($\gamma = -0.149$ cm^{-1} in the case of NiF and $\gamma = -0.115$ cm^{-1} in the case of NiCl). The main contribution to the γ value is the second-order spin–orbit interaction with neighboring Π states of the same multiplicity (*10, 11*). It is tempting to test the pure-precession relationship (*12*)

$$\gamma = \frac{2AB l(l+1)}{E_\Pi - E_\Sigma},$$

assuming that the $^2\Sigma^+$ state interacts with the $X^2\Pi_i$ state. As the $X^2\Pi_i$ state is an inverted state, it is obvious that γ must be positive. If we suppose that the $X^2\Pi_i$ and the $[1.7]A^2\Sigma^+$ states of NiCl form a unique perturber pair, the negative experimental value of γ for the $^2\Sigma^+$ states of NiF and NiCl does not fulfill

TABLE 3
Molecular Constants (in cm^{-1}) for the $[24.9]^2\Pi_{1/2}$ ($v = 0$), $[24.5]^2\Pi_{3/2}$ ($v = 0$), and $[1.7]^2\Sigma^+$ ($v = 0$) States of ^{58}Ni^{35}Cl (All Uncertainties are 1σ)

State	T_0	A_0	B_0	$D_0 \times 10^7$	p_0	γ_0	$\gamma_D \times 10^7$
$[24.9]^2\Pi_{1/2}$	24732.873(2)	−484.545(2)	0.174628(10)	1.181(11)	−0.01996(7)		
$[24.5]^2\Pi_{3/2}$			0.174781(10)				
$[1.7]^2\Sigma^+$	1768.070(2)		0.179848(10)	0.982(20)		−0.11541(8)	10.43 (30)

TABLE 4
Bandhead Positions (in cm^{-1}) of the Vibrational Bands Identified for the Observed Electronic Transitions

Transition	v' – v "	ν_{head} (cm^{-1})	Transition	v' – v "	ν_{head} (cm^{-1})
$[24.5]^2\Pi_{3/2} - X^2\Pi_{3/2}$	0 – 0	24 495.1	$[24.9]^2\Pi_{1/2} - X^2\Pi_{3/2}$	0 – 0	24 980.3
	1 – 1	24 478.0			
	2 – 2	24 460.3			
	1 – 0	24 899.8			
	0 – 1	24 073.3			
$[24.5]^2\Pi_{3/2} - [0.16]^2\Delta_{5/2}$	0 – 0	24 332.4			
	1 – 1	24 305.5			
	1 – 0	24 737.4			
	0 – 1	23 900.7			
$[24.5]^2\Pi_{3/2} - [1.7]^2\Sigma^+$	0 – 0	22 738.8 ($^SR_{ee}$)	$[24.9]^2\Pi_{1/2} - [1.7]^2\Sigma^+$	0 – 0	23 223.1 (R_{ee})
	1 – 1	22 718.4 ($^SR_{ee}$)		1 – 1	23 201.0 (R_{ee})
	2 – 2	22 697.8 ($^SR_{ee}$)		2 – 2	23 178.2 (R_{ee})
				1 – 0	23 624.0 (R_{ee})

this hypothesis. The isoelectronic molecule CuO follows the same behavior (*13*). The $Y^2\Sigma^+$ state located 7715 cm^{-1} above the ground $X^2\Pi_i$ state is also characterized by a negative γ parameter (-0.089587 cm^{-1}), similar in magnitude to the values for the $^2\Sigma^+$ states of NiF and NiCl. For all these molecules we suspect that other doublet or quartet states are nearby and contribute to a negative value for γ. In the case of NiF, we have located (252 cm^{-1} above the ground $X^2\Pi_{3/2}$ state) a so-called "$^2\Sigma^+$" state characterized by a very large γ parameter (-0.952 cm^{-1}) (*2*). This large negative value has been confirmed by microwave experiments (*14*). It is not out of the question that this state could be the expected $^2\Pi_{1/2}$ spin–orbit component of the ground state, strongly influenced by unidentified states. (Note that a new group of states has been identified (*15*) but not included in the energy level diagram of the doublet states of NiF.) This supports the idea that the energy level diagram of the lower states of NiF and NiCl is not yet complete.

Along with the identification of the $^2\Delta_{3/2}$ spin–orbit component of $A^2\Delta_i$ state, the identification of the $^2\Pi_{1/2}$ spin component of the $X^2\Pi_i$ is of interest to see if, as observed for NiF, it is strongly perturbed.

ACKNOWLEDGMENTS

The Centre d'Etudes et de Recherches Lasers et Applications is supported by the Ministère Chargé de la Recherche, the Région Nord-Pas de Calais, and the Fond Européen de Développement Economique des Régions. This work was supported by the Natural Sciences and Engineering Research Council of Canada (NSERC). Acknowledgment is also made to the Petroleum Research Fund for partial support.

REFERENCES

1. T. Hirao, C. Dufour, B. Pinchemel, and P. F. Bernath, *J. Mol. Spectrosc.* **202,** 53–58 (2000).
2. C. Dufour and B. Pinchemel, *J. Mol. Spectrosc.* **173,** 70–78 (1995).
3. P. Carette, C. Dufour, and B. Pinchemel, *J. Mol. Spectrosc.* **161,** 323–335 (1993).
4. B. Edlén, *Metrologia* **2,** 71–80 (1966).
5. K. P. Birch and M. J. Downs, *Metrologia* **30,** 155–162 (1993).
6. T. Hirao, B. Pinchemel, and P. F. Bernath, *J. Mol. Spectrosc.* **202,** 213–222 (2000).
7. G. Norlén, *Phys. Scr.* **8,** 249–268 (1973).
8. G. Herzberg, "Spectra of Diatomic Molecules," Van Nostrand, Princeton, 1950.
9. A. J. Kotlar, R. W. Field, and J. I. Steinfeld, *J. Mol. Spectrosc.* **80,** 86–108 (1980).
10. J. H. VanVleck, *Rev. Mod. Phys.* **23,** 213–227 (1951).
11. R. S. Mulliken and A. Christy, *Phys Rev.* **38,** 87–119 (1931).
12. H. Lefebvre-Brion and R. W. Field, "Perturbations in the Spectra of Diatomic Molecules," Academic Press, San Diego, 1986.
13. L. C. O'Brien, R. L. Kubicek, S. J. Wall, D. E. Koch, R. J. Friend, and C. R. Brazier, *J. Mol. Spectrosc.* **180,** 365–368 (1996).
14. T. Okabayashi and M. Tanimoto, private communication.
15. C. Focsa, C. Dufour, and B. Pinchemel, *J. Mol. Spectrosc.* **182,** 65–71 (1997).